# Loss of memory of an elastic line on its way to limit cycles

Elisabeth Agoritsas, Jonathan Barés

Letter

# Loss of memory of an elastic line on its way to limit cycles

Elisabeth Agoritsas[1,*] and Jonathan Barés[2,†]

[1]*Department of Quantum Matter Physics (DQMP), University of Geneva, Quai Ernest-Ansermet 24, CH-1211 Geneva, Switzerland*

[2]*Laboratoire de Mécanique et Génie Civil (LMGC), UMR 5508 CNRS-University Montpellier, 34095 Montpellier, France*

(Received 10 August 2023; accepted 10 March 2024; published 1 April 2024)

Oscillatory-driven amorphous materials forget their initial configuration and converge to limit cycles. Here we investigate this memory loss under a nonquasistatic drive in a minimal model system, with quenched disorder and memory encoded in a spatial pattern, where oscillating protocols are formally replaced by a positive-velocity drive. We consider an elastic line driven athermally in a quenched disorder with biperiodic boundary conditions and tunable system size, thus controlling the area swept by the line per cycle as would the oscillation amplitude. The convergence to disorder-dependent limit cycle is strongly coupled to the nature of its velocity dynamics depending on system size. Based on the corresponding phase diagram, we propose a generic scenario for memory formation in disordered systems under finite driving rate.

DOI: 10.1103/PhysRevE.109.L042901

*Introduction.* Theoretical descriptions of driven amorphous materials remain challenging, both for the rheology of yield stress fluids [1] or the mechanics of structural glasses [2]. Part of their complexity stems from their structural disorder—self-generated by the relative position of their individual constituents—which plays a key role in their response to an external drive. There has been recently a collective endeavor to revisit the prominent features of these materials from the prism of memory formation [3,4]. Characterizing transient regimes, toward steady-state or hysteretic behaviors, amounts to study how materials forget an initial configuration and eventually "learn" a new driving-dependent state. The encoding and retrieval of such memories in amorphous materials is a promising avenue for metamaterials development [5,6].

In that respect, oscillatory protocols play a special role. By tuning their amplitude, period, and spatial pattern, they allow us to systematically probe the explored disordered landscape. Thermal activation is ill controlled in comparison, probing energy barriers in a random and statistically isotropic way. On the numerical side, the oscillatory-athermal-quasistatic-shear (OAQS) protocols provide bare characterizations of the landscape features with no characteristic timescale [7]. They have been the focus of several recent studies, either in particle-based [8–12] or coarse-grained models [13–16]. Microscopically, an amorphous material experiences plastic events, which locally update the structural disorder and generate a mechanical noise. Upon this iterative restructuring, and depending on the driving amplitude, the material response departs from an initial elastic regime, and after one or several oscillatory cycles converges into a hysteretic behavior. Remarkably, the complex structure of these transient and limit-cycle responses upon OAQS can further be revealed via random transition graphs between mechanically stable configurations [17–20]. On the experimental side, however, oscillatory protocols are often performed at a finite driving rate, typically with a sinusoidal shear strain (or stress), whose frequency dependence is central in rheological measurements of storage and loss moduli [1,21–24]. The additional timescale introduced by the drive compels us to clarify the interplay between elastic relaxation and disorder dynamics. In particular, it questions the generalizability of the memory picture built on quasistatic protocols to actual rheological experiments, already at a formal level.

In this Letter, we investigate numerically a minimal model system, devised to disentangle these memory effects from the structural disorder dynamics, focusing on displacement-controlled protocols at finite velocity. It aims to bypass three main difficulties: first, in amorphous materials, configurations and disorder are parametrized by the same degrees of freedom, namely the positions of individual particles; second, we are better equipped theoretically to address overdamped steady states at positive driving, rather than hysteretic behaviors under oscillating protocols; third, a bidimensional system permits direct visualization of what happens, especially for the memory process, and faster simulations. Our model system consists of an elastic line driven athermally in a biperiodic 2D random landscape by adjusting the center-of-mass velocity. The disorder is quenched with *ad hoc* features that we fully control. Memory is encoded in the geometrical and velocity profiles of the line, and oscillating protocols are formally replaced by a positive velocity drive: instead of driving the line back and forth swiping repeatedly the same landscape, the line is continuously driven over a repeated landscape. Hence, tuning the system size controls the area swept by the line per cycle, as would an oscillatory amplitude.

Our findings put forward the key role of velocity dynamics regarding memory formation. In the absence of thermal fluctuations, the line converges to disorder-dependent limit cycles. In quasistatic, the limit cycle is then fully characterized by the sole shape of the line, optimized in the successive minima

*elisabeth.agoritsas@unige.ch

†jonathan.bares@umontpellier.fr

 

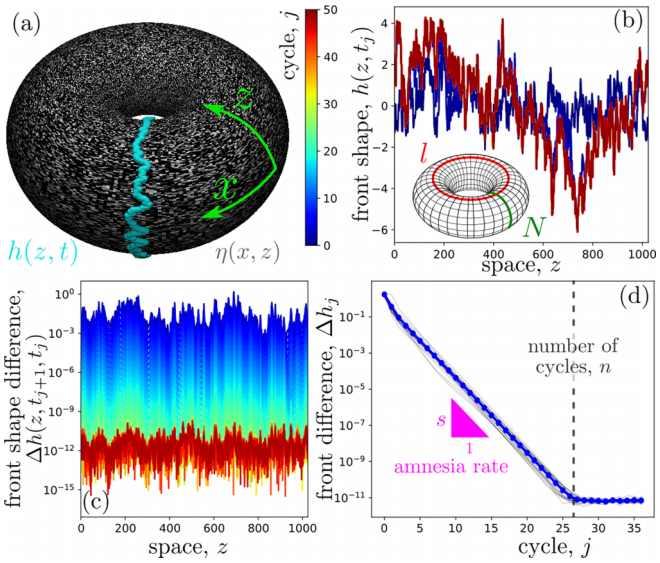


FIG. 1. Settings: (a) Quenched disorder $\eta(x,z)$ embedded in a biperiodic 2D space of coordinates $(x,z) \in [0,\ell] \times [0,N]$; driven elastic line parametrized by the univalued profile $h(z,t)$. (b) Stroboscopic view of its geometrical profile when $\bar{h}(t_j) = 0$. (c) Profile difference, in absolute value, between successive cycles. (d) Exponential decay of the integrated profile difference $\Delta h_j$, plateauing after $n$ cycles. Parameters: $c = 10^{-3}$, $k = 10^{-2}$, $\sigma = 1$, $N = 1024$, $l = 10$.

of the disordered landscape. For a finite driving rate, on the contrary, part of the memory is encoded in the velocity profile. Therefore, the way the system forgets its initial conditions will also strongly depend on the nature of the velocity dynamics, self-consistently fixed by the disorder/size/driving settings.

*Model.* We consider an elastic line evolving in a 2D space of coordinates $(x,z) \in [0,\ell] \times [0,N]$ with biperiodic boundary conditions, as shown in Fig. 1(a). In the absence of overhangs, this front shape is parametrized by an univalued profile $h(z,t)$. It evolves in a quenched random field $\eta(x,z)$, with the overdamped dynamics

$$\partial_t h(z,t) = \underbrace{ct - k\langle h(z,t)\rangle_z}_{\text{speed loading, } F_{\text{load}}} + \underbrace{F_{\text{st}}[h(z,t)]}_{\text{stiffness}} + \underbrace{\sigma\,\eta(h(z,t),z)}_{\text{disorder}}$$

$$\text{with} \quad F_{\text{st}}[h(z,t)] = \frac{1}{\pi}\int_0^N \mathrm{d}z'\,\frac{h(z',t)-h(z,t)}{|z'-z|^{\gamma}} \tag{1}$$

with the loading rate $c$, unloading factor $k$, and disorder amplitude $\sigma$. $\langle\bullet\rangle_z$ denotes the spatial average in the $z$ direction, hence $\langle h(z,t)\rangle_z \equiv \bar{h}(t)$ is the center of mass. We assume a Gaussian disorder of zero means, denoting $\overline{\bullet}$ the average over disorder realisations, $\overline{\eta(x,z)} = 0$ and $\overline{\eta(x,z)\eta(x',z')} = 2\,\delta(x-x')\delta(z-z')$, i.e., spatially uncorrelated above the numerical discretization scale. The "stiffness" elasticity range can be tuned by changing the exponent $\gamma$, and to focus for now on a single model here we set $\gamma = 2$. The remaining parameters are tuned to probe the different amnesia regimes : $c \in [10^{-5}, 5\times10^{-2}]$, $k \in [10^{-3}, 5\times10^{-1}]$, $\sigma \in [0.1, 5]$, and in pixel-size units $N \in [128, 16384]$ and $l \in [2, 400]$.

This is one representative example of the theoretical framework of disordered elastic systems, successfully applied to a broad range of physical interfaces (ferroic domain walls, imbibition, proliferating cells fronts, etc.) to address the role of disorder in their properties [25–29]. We focus on the long-range elastic line ($\gamma = 2$) with "random-field" disorder, extensively investigated as a paradigm of brittle cracks in fracture mechanics [30–37]. It is also relevant for driven amorphous materials, as it retains the long-range nature of the Eshelby stress propagator (recognized as key to amorphous plasticity), albeit without its nonconvex features [38,39]. Moreover, our driving is formally closer to a genuine mechanical loading. Our model's critical features in the steady state are well benchmarked within the depinning formalism [34,40–43], allowing us to focus directly on memory issues. In a nutshell, (i) The speed loading $F_{\text{load}}(t)$ is a competition between an external loading rate $c$ and a restoring stiffness $k$ acting on the center of mass. This displacement-controlled driving guarantees that the line will always reach a finite steady velocity and $F_{\text{load}}^{\text{steady}}(t) \geqslant F_c$, where $F_c$ is a critical force set by the disorder configuration [44]. (ii) Conversely, in an athermal constant force driving, $F_c$ is the minimal force needed to reach such a self-sustained steady state. (iii) The nature of the velocity dynamics changes radically depending on the proximity to $F_c$: in the "fast-flow" or continuous regime, the average velocity displays small fluctuations around the mean $c/k$, i.e., $F_{\text{load}}^{\text{steady}}(t) \approx c/k \gg F_c$; closer to $F_c$, the line advances intermittently via critical avalanches, in the so-called "crackling" regime [34]. These features are generic for many driven disordered systems, and reminiscent of the yielding transition of amorphous materials [38,39,45].

Regarding the present study, we could have considered alternative choices for the elasticity and disorder, similarly benchmarked. Yet, with our choice we anticipate reintroducing disorder dynamics in our model system: [43] provides an additional benchmark on how artificial disorder updates trigger avalanches and modify their distributions in a controlled way.

*Memory characterization.* The transverse size $\ell$ is usually considered as a necessary nuisance in numerical simulations [46], whereas here it is precisely our control parameter of interest. We start with a flat and still initial condition ($h(z,0) = \partial_t h(z,0) = 0\,\forall z$), and drive deterministically the line at finite rate with its overdamped dynamics over $j$ cycles in the $x$ direction. We take a stroboscopic snapshot of its shape each time $t_j$ its center of mass crosses $x = 0$. We then quantify the convergence to a limit cycle, for a given disorder realization, by comparing consecutive profiles $h_j(z) \equiv h(z,t_j)$. These are typically quite close [see Fig. 1(b)], thus we focus instead on their front shape difference

$$\Delta h(z,t_{j+1},t_j) \equiv |h(z,t_{j+1}) - h(z,t_j)|,$$

$$\Delta h_j \equiv \langle \Delta h(z,t_{j+1},t_j)\rangle_z = \frac{1}{N}\int_0^N \mathrm{d}z\,\Delta h(z,t_{j+1},t_j), \tag{2}$$

as shown in Figs. 1(c) and 1(d). By plotting the average difference as a function of the cycles, we can follow the memory loss and convergence to a limit cycle. See the Supplemental Material (SM) [47] for alternative criteria, including the

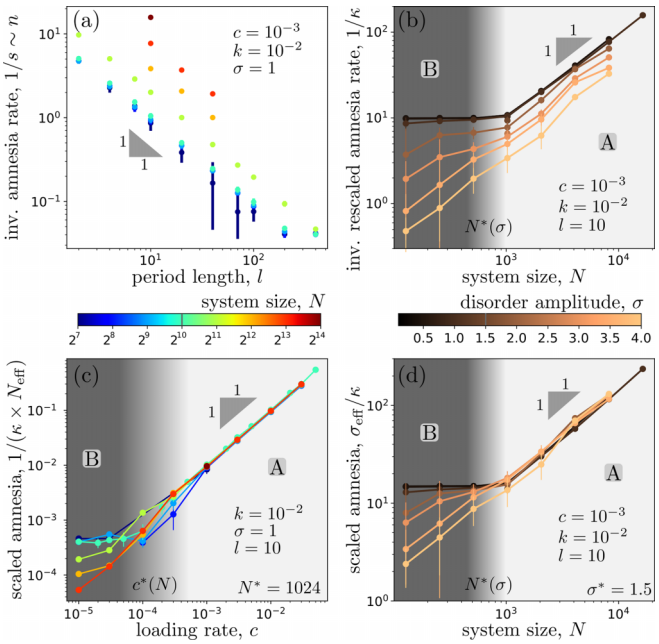


FIG. 2. Quantifying amnesia: (a) Inverse amnesia rate $1/s \sim n$ as a function of transverse size $\ell$, for different system size $N$. (b) Proxy for the distance to amnesia, $1/\kappa$, as a function of $N$, for different disorder amplitude $\sigma$. For small $\sigma$, two distinct regimes separated by $N^*(\sigma)$ are highlighted with gray shading (**A**-right, **B**-left). (c) Inverse amnesia rates as a function of the loading rate $c$ for different system size $N$. Collapse in **A** is obtained upon rescaling with $N_{\rm eff}(N > N^*) = N$ and $N_{\rm eff} \approx N^*$ otherwise; this reveals a crossover at loading $c^*(N)$ highlighted in gray shading. (d) Partial collapse in **A** of (b) upon rescaling with $\sigma_{\rm eff}(\sigma > \sigma^*) = \sigma$ and $\sigma_{\rm eff} \approx \sigma^*$ otherwise. Error bars are for disorder fluctuations.

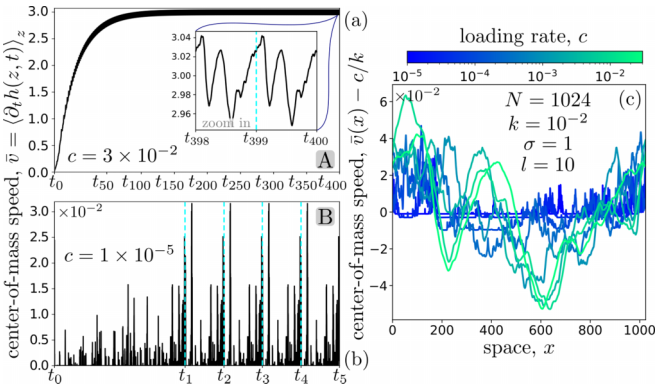


FIG. 3. Center-of-mass dynamics: (a), (b) Evolution of the center-of-mass speed $\bar{v}(t)$ for fast (**A**) and slow (**B**) loading, matching the two regimes in Fig. 2(a). Times $\{t_j\}$ when the system begins a new cycle are given on the horizontal axis. (c) Center-of-mass speed $\bar{v}(x)$ along a cycle in the converged regime for increasing speed rate, for the same disorder and initial condition. Data are shifted by the average speed $c/k$, and mapped on the spatial interval $x(t) \in [0, \ell]$.

velocity profiles $v_j(z) \equiv \partial_t h(z, t_j)$, supporting that we can safely focus on the most straightforward indicator, $\Delta h_j$.

As shown in Fig. 1(d), the qualitative trend is an exponential decrease of $\Delta h_j$ until it plateaus. We aim to understand what controls the number of cycles $n$ needed to reach the plateau $\Delta h_\infty$. The latter would be strictly zero if the line was reaching a unique limit cycle, as expected in an athermal quasistatic driving by Middleton's theorem [48], assuming a perfect numerical resolution. In practice, the key quantity to extract is the average slope of $\Delta h_j$ in semilog scale, i.e., the amnesia rate $s \approx -\partial_j \log \Delta h_j$. For an exponential decrease $\Delta h_{(j \leqslant n)} = Ae^{-sj}$ and a negligible plateau, we have $n = -\log(\Delta h_\infty / A)/s \approx \log(A)/s$ where $A$ depends on the initial condition. The inverse amnesia rate is a good proxy for the number of cycles ($n \sim s^{-1}$), much less sensitive to initial conditions and independent of the plateau value (see the SM). The figures reported here are based on this quantity.

*Number of cycles for amnesia.* For the considered parameter range, the plateau value $\Delta h_\infty \approx 10^{-13}$ is fixed by the numerical resolution and thus negligible. Keeping the parameters $\{c, k, \sigma\}$ fixed, we find that $n$ decreases linearly in the transverse size $\ell$ [see Fig. 2(a)]. This suggests to consider instead $d_n = n\ell$, i.e., the distance covered by the center of mass to reach amnesia, and we focus on the rescaled amnesia rate defined as $\kappa = s/\ell \sim d_n^{-1}$. By plotting this proxy for $d_n$ with respect to $N$ [see Fig. 2(b)], two distinct regimes arise for the small $\sigma$: linear above a given $N^*(\sigma)$ (**A**, pale region) and constant below (**B**, dark region). Above $N^*$, the number of cycles for amnesia is proportional to the aspect ratio of the system size: $\kappa^{-1} \sim d_n \sim N$, thus $n \sim N/\ell$. In **A**, memory is extensive. Below $N^*$, the distance $d_n$ saturates at $d_n \sim N^*(\sigma)$. In **B**, there is a minimal distance required to forget, which can only depend on the remaining parameters. Under a quasistatic drive, $d_n$ must be fixed by the landscape features ($\sigma$), whereas at finite driving it may also depend on how fast the line is driven ($c, k$).

*Amnesia rate vs loading and disorder.* To further understand how the memory extensivity is broken, we thus vary independently $\{c, \sigma\}$, while imposing $k = 0.01$ without any loss of generality. In Fig. 2(b), regimes **A** and **B** were clearly distinct for small $\sigma$ on which the gry shading is based, whereas upon increasing disorder, the data spread and render the saturation toward **B**, less apparent in log scale. We thus focus on comparing curves where memory is extensive and rescale them such as to collapse their **A** regime. Figures 2(c) and 2(d) suggest the existence of characteristic $c^*$ and $1/\sigma^*$, respectively, below which the amnesia regime departs from $\kappa^{-1} \sim c/\sigma$.

These linear scalings and crossovers are not to be taken as robust characterizations, they merely highlight the general trend: memory is extensive as long as the disorder is weak (below $\sigma^*$), the system is large (above $N^*$), or the driving is fast (above $c^*$). In **A** the number of cycles $n \approx s^{-1} \sim (N/\ell)(c/\sigma)$ implies in particular that it takes fewer cycles to converge to the limit cycle at lower loading. We eventually depart from this regime at $c < c^*(N, \ell, \sigma)$, which includes the quasistatic limit. This strongly suggests examining the velocity dynamics associated with these different behaviors.

*Relevance of the velocity dynamics.* The velocity profiles also converge to limit cycles (see the SM), yet the center-of-mass speed $\bar{v}(t)$ is more informative on what happens within each cycle. The left of Fig. 3 illustrates two very distinct behaviors, as expected from previous studies [34]: **A** converges to a continuous regime in the limit cycle, and **B** to an intermittent behavior. The only difference between these two

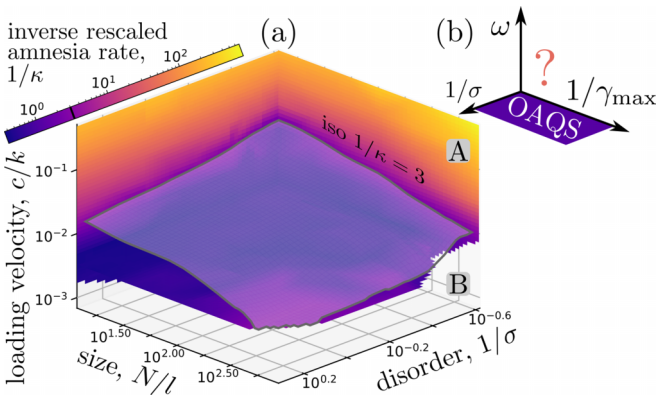


FIG. 4. Phase diagram of memory formation vs nature of the velocity dynamics: continuous (**A**) above the isosurface and intermittent (**B**) below. The isosurface $\kappa = 1/3$ is an arbitrary threshold, below which $\kappa$ mainly saturates. See the SM for an animated plot.

cases is the loading rate, with **A** at $c > c^*(N)$ and **B** otherwise. In Fig. 3(c) we further show how varying the loading rate modifies the limit cycle for $\bar{v}(t)$, for a given disordered landscape.

These findings support the following scenario: For a given landscape of parameters $\{N, \ell, \sigma\}$, the finite speed loading $\{c, k\}$ determines if the dynamics in the limit cycle are either continuous ($\bar{v} \approx c/k$ with small fluctuations) or intermittent (but always strictly positive). The associated transient regime from flat initial conditions will share similar qualitative features. In the continuous case (**A**) the line is driven so fast that it flies over the landscape, without fully relaxing in its minima; it consequently needs more cycles to learn its features, its amnesia rate is smaller, and memory is extensive ($d_n \sim N$). In the intermittent case (**B**), the line is driven so slowly that it follows closely the landscape; disorder features are encoded more efficiently, i.e., in less cycles, amnesia rate is larger, and extensivity is broken.

*Unifying phase diagram.* For such disordered elastic systems, the crossover between these two types of behaviors is highly nontrivial for steady states [26,34,37], and *a fortiori* for transient regimes. To support our scenario, we plot in Fig. 4 the rescaled amnesia rates $\kappa \sim 1/(n\ell)$ through the 3D phase space of our minimal model. The three axes control the aspect ratio $N/\ell$, the inverse amplitude of disorder, and the forcing $c/k$. For each point, we can discriminate between continuous (**A**) or intermittent (**B**) transient behaviors, albeit with a quantitative dependence on the thresholding (see the SM). It is consistent with the saturation of $\kappa$ highlighted by the isosurface $\kappa = 1/3$, confirming our physical picture. This phase diagram thus rationalizes the memory formation at finite driving rate, in a tunable disordered landscape.

*Insights for driven amorphous materials.* A genuine oscillatory protocol at finite velocity amounts to replace in Eq. (1) the loading by a sinusoidal force, of amplitude $\gamma_{\max}$ and frequency $\omega$ [28,49–52]. In our model, $\gamma_{\max}$ translates formally into the aspect ratio $\ell/N$, and $\omega$ into the loading $v = c/k$. According to our phase diagram, increasing $\gamma_{\max}$ or decreasing $\omega$ is expected to radically change the memory formation, making it more efficient (fewer cycles), with a crossover from continuous to intermittent dynamics [53]. The precise location in this diagram will further depend on the disorder strength $\sigma$. For amorphous materials, the latter is self-consistently determined for a given driving protocol, and *a priori* not constant in transient regimes. This implies that, in order to rationalize memory formation under nonquasistatic oscillating protocols, one would crucially need to characterize jointly the driving-dependent disorder strength and the resulting nature of the velocity dynamics at fixed $\{\omega, \gamma_{\max}\}$.

The well-studied OAQS regime corresponds to a plane of our putative phase diagram, as sketched in Fig. 4. Adding a finite driving rate is bound to unveil a more complex behavior, as already displayed by our minimal model with frozen disorder dynamics. Here we showed that driven disordered systems can display very different memory behavior, and traced this back to how the velocity dynamics is self-consistently fixed by the disorder/size/driving settings. This is the core of the depinninglike phenomenology, hence this scenario should hold more broadly for disordered elastic systems. By construction, our specific model system is not expected to reproduce the full phenomenology of oscillatory-driven amorphous materials, first and foremost because it does not include the nonconvex features of the Eshelby kernel. Yet, the analogy between the depinning and yielding transitions in coarse-grained models [38,39,45], which generically display such a transition from continuous versus intermittent velocity dynamics, strongly suggests challenging our generic scenario already at this level.

*Concluding remarks.* We started from a flat configuration and examined how the line converges, at finite driving rate, to its limit cycle jointly for its geometric and velocity profiles. Focusing on the rescaled amnesia rate $\kappa$, we find that there is a regime where the memory is extensive, i.e., $\kappa^{-1}$ is proportional to the system size $N$, the loading, and the inverse of the disorder amplitude. It requires more cycles to "learn" the quenched landscape when the latter is small or the line is driven faster. If we start from a configuration closer to the limit cycle, this number of cycles will be reduced accordingly. On the contrary, the amnesia rate will not be affected, promoting it to the key physical quantity to follow in further studies, and in particular to investigate the intermittent regime where $\kappa$ saturates.

The scenario we put forward is generic for an extended object driven repeatedly over a given patch of disordered landscape, until the geometry of this object fully encodes the finite amount of information associated with the disorder. The specific scalings will of course vary on the microscopic model, for instance, we expect the memory extensivity to generalize to $n \sim N/\ell^{f(\gamma)}$ when tuning the elasticity range. In this regime, the limit cycles correspond to the so-called fast-flow regime in "random-periodic" disorder settings [46], thus paving the way for an analytical study of transient regimes [54].

Finally, our minimal model system provides a controlled framework to systematically investigate the joint role of initial conditions and disorder features in memory formation. In addition to allowing for a finite spatial correlation length [55,56] and/or a more complex hierarchical structure of the landscape [57], two key ingredients to address in the future are tunable disorder dynamics as in [43] and different initial conditions. Both could be tailored to mimic the self-consistent disorder

dynamics in driven amorphous materials, in order to probe its relevance for memory in finite driving protocols [58,59].

*Acknowledgments.* We thank Muhittin Mungan, Alberto Rosso, and Damien Vandembroucq for fruitful discussions. E.A. acknowledges support from the Swiss National Science Foundation by the SNSF Ambizione Grant No. PZ00P2_-173962, and from the Simons Foundation (Grant No. 348126 to Sidney Nagel).

[1] D. Bonn, M. M. Denn, L. Berthier, T. Divoux, and S. Manneville, Yield stress materials in soft condensed matter, Rev. Mod. Phys. **89**, 035005 (2017).

[2] F. Arceri, F. P. Landes, L. Berthier, and G. Biroli, Glasses and aging: A statistical mechanics perspective, Encyclopedia of Complexity and Systems Science, arXiv:2006.09725.

[3] N. C. Keim, J. D. Paulsen, Z. Zeravcic, S. Sastry, and S. R. Nagel, Memory formation in matter, Rev. Mod. Phys. **91**, 035002 (2019).

[4] S. R. Nagel, S. Sastry, Z. Zeravcic, and M. Muthukumar, Memory formation, J. Chem. Phys. **158**, 210401 (2023).

[5] M. Kadic, G. W. Milton, M. van Hecke, and M. Wegener, 3D metamaterials, Nat. Rev. Phys. **1**, 198 (2019).

[6] S. Yu, C.-W. Qiu, Y. Chong, S. Torquato, and N. Park, Engineered disorder in photonics, Nat. Rev. Mater. **6**, 226 (2021).

[7] C. E. Maloney and A. Lemaître, Amorphous systems in athermal, quasistatic shear, Phys. Rev. E **74**, 016118 (2006).

[8] T. Kawasaki and L. Berthier, Macroscopic yielding in jammed solids is accompanied by a nonequilibrium first-order transition in particle trajectories, Phys. Rev. E **94**, 022615 (2016).

[9] P. Leishangthem, A. D. S. Parmar, and S. Sastry, The yielding transition in amorphous solids under oscillatory shear deformation, Nat. Commun. **8**, 14653 (2017).

[10] M. Adhikari and S. Sastry, Memory formation in cyclically deformed amorphous solids and sphere assemblies, Eur. Phys. J. E **41**, 105 (2018).

[11] W.-T. Yeh, M. Ozawa, K. Miyazaki, T. Kawasaki, and L. Berthier, Glass stability changes the nature of yielding under oscillatory shear, Phys. Rev. Lett. **124**, 225502 (2020).

[12] H. Bhaumik, G. Foffi, and S. Sastry, The role of annealing in determining the yielding behavior of glasses under cyclic shear deformation, PNAS **118**, e2100227118 (2021).

[13] K. Khirallah, B. Tyukodi, D. Vandembroucq, and C. E. Maloney, Yielding in an integer automaton model for amorphous solids under cyclic Shear, Phys. Rev. Lett. **126**, 218005 (2021).

[14] D. Kumar, S. Patinet, C. E. Maloney, I. Regev, D. Vandembroucq, and M. Mungan, Mapping out the glassy landscape of a mesoscopic elastoplastic model, J. Chem. Phys. **157**, 174504 (2022).

[15] C. Liu, E. E. Ferrero, E. A. Jagla, K. Martens, A. Rosso, and L. Talon, The fate of shear-oscillated amorphous solids, J. Chem. Phys. **156**, 104902 (2022).

[16] J. T. Parley, S. Sastry, and P. Sollich, Mean-field theory of yielding under oscillatory shear, Phys. Rev. Lett. **128**, 198001 (2022).

[17] M. Mungan and T. A. Witten, Cyclic annealing as an iterated random map, Phys. Rev. E **99**, 052132 (2019).

[18] M. Mungan, S. Sastry, K. Dahmen, and I. Regev, Networks and hierarchies: How amorphous materials learn to remember, Phys. Rev. Lett. **123**, 178002 (2019).

[19] I. Regev, I. Attia, K. Dahmen, S. Sastry, and M. Mungan, Topology of the energy landscape of sheared amorphous solids and the irreversibility transition, Phys. Rev. E **103**, 062614 (2021).

[20] M. Mungan and S. Sastry, Metastability as a mechanism for yielding in amorphous solids under cyclic shear, Phys. Rev. Lett. **127**, 248002 (2021).

[21] N. C. Keim and J. D. Paulsen, Multiperiodic orbits from interacting soft spots in cyclically sheared amorphous solids, Sci. Adv. **7**, eabg7685 (2021).

[22] D. Wang, J. A. Dijksman, J. Barés, J. Ren, H. Zheng, Sheared amorphous packings display two separate particle transport mechanisms, Phys. Rev. Lett. **125**, 138001 (2020).

[23] Y. Zhao, Y. Zhao, D. Wang, H. Zheng, B. Chakraborty, and J. E. S. Socolar, Ultrastable shear-jammed granular material, Phys. Rev. X **12**, 031021 (2022).

[24] Y. Xing, J. Zheng, J. Li, Y. Cao, W. Pan, J. Zhang, and Y. Wang, X-ray tomography investigation of cyclically sheared granular materials, Phys. Rev. Lett. **126**, 048002 (2021).

[25] E. Agoritsas, V. Lecomte, and T. Giamarchi, Disordered elastic systems and one-dimensional interfaces, Physica B: Condens. Matter **407**, 1725 (2012).

[26] K. J. Wiese, Theory and experiments for disordered elastic manifolds, depinning, avalanches, and sandpiles, Rep. Prog. Phys. **85**, 086502 (2022).

[27] D. S. Fisher, Collective transport in random media: From superconductors to earthquakes, Phys. Rep. **301**, 113 (1998).

[28] S. Brazovskii and T. Nattermann, Pinning and sliding of driven elastic systems: From domain walls to charge density waves, Adv. Phys. **53**, 177 (2004).

[29] S. Santucci, R. Planet, K. J. Måløy, and J. Ortín, Avalanches of imbibition fronts: Towards critical pinning, Europhys. Lett. **94**, 46005 (2011).

[30] A. Tanguy, M. Gounelle, S. Roux, From individual to collective pinning: Effect of long-range elastic interactions, Phys. Rev. E **58**, 1577 (1998).

[31] K. J. Måløy, S. Santucci, J. Schmittbuhl, and R. Toussaint, Local waiting time fluctuations along a randomly pinned crack front, Phys. Rev. Lett. **96**, 045501 (2006).

[32] M. J. Alava, P. K. V. V. Nukala, and S. Zapperi, Statistical models of fracture, Adv. Phys. **55**, 349 (2006).

[33] L. Ponson and D. Bonamy, Crack propagation in brittle heterogeneous solids: Material disorder and crack dynamics, Int. J. Fract. **162**, 21 (2010).

[34] J. Barés, L. Barbier, and D. Bonamy, Crackling versus continuumlike dynamics in brittle failure, Phys. Rev. Lett. **111**, 054301 (2013).

[35] J. Barés, A. Dubois, L. Hattali, D. Dalmas, and D. Bonamy, Aftershock sequences and seismic-like organization of acoustic events produced by a single propagating crack, Nat. Commun. **9**, 1253 (2018).

[36] J. Barés and D. Bonamy, Crack growth in heterogeneous brittle solids: intermittency, crackling and induced

seismicity, Philos. Trans. R. Soc. A **377**, 20170386 (2019).
[37] J. Barés, D. Bonamy, and A. Rosso, Seismiclike organization of avalanches in a driven long-range elastic string as a paradigm of brittle cracks, Phys. Rev. E **100**, 023001 (2019).
[38] J. Lin, E. Lerner, A. Rosso, and M. Wyart, Scaling description of the yielding transition in soft amorphous solids at zero temperature, Proc. Natl. Acad. Sci. USA **111**, 14382 (2014).
[39] B. Tyukodi, S. Patinet, S. Roux, and D. Vandembroucq, From depinning transition to plastic yielding of amorphous media: A soft-modes perspective, Phys. Rev. E **93**, 063005 (2016).
[40] D. Ertaş and M. Kardar, Critical dynamics of contact line depinning, Phys. Rev. E **49**, R2532 (1994).
[41] V. Démery, A. Rosso, and L. Ponson, From microstructural features to effective toughness in disordered brittle solids, Europhys. Lett. **105**, 34003 (2014).
[42] V. Démery, V. Lecomte, and A. Rosso, The effect of disorder geometry on the critical force in disordered elastic systems, J. Stat. Mech. (2014) P03009.
[43] J. Barés and D. Bonamy, Controlling crackling dynamics by triggering low-intensity avalanches, Phys. Rev. E **103**, 053001 (2021).
[44] C. J. Bolech and A. Rosso, Universal statistics of the critical depinning force of elastic systems in random media, Phys. Rev. Lett. **93**, 125701 (2004).
[45] J.-C. Baret, D. Vandembroucq, and S. Roux, Extremal model for amorphous media plasticity, Phys. Rev. Lett. **89**, 195506 (2002).
[46] S. Bustingorry, A. B. Kolton, and T. Giamarchi, Random-manifold to random-periodic depinning of an elastic interface, Phys. Rev. B **82**, 094202 (2010).
[47] See Supplemental Material at http://link.aps.org/supplemental/10.1103/PhysRevE.109.L042901 for a presentation of the data in a more exhaustive way while providing more details about the numerical recipes.
[48] A. A. Middleton, Asymptotic uniqueness of the sliding state for charge-density waves, Phys. Rev. Lett. **68**, 670 (1992).
[49] T. Nattermann, V. Pokrovsky, and V. M. Vinokur, Hysteretic dynamics of domain walls at finite temperatures, Phys. Rev. Lett. **87**, 197005 (2001).
[50] A. Glatz, T. Nattermann, and V. Pokrovsky, Domain wall depinning in random media by ac fields, Phys. Rev. Lett. **90**, 047201 (2003).
[51] F. Schütze, Perturbation theory for ac-driven interfaces in random media, Phys. Rev. E **81**, 051128 (2010).
[52] F. Schütze and T. Nattermann, Mean-field theory for driven domain walls in disordered environments, Phys. Rev. B **83**, 024412 (2011).
[53] A. Abed Zadeh, J. Barés, and. P. Behringer, Crackling to periodic dynamics in granular media, Phys. Rev. E **99**, 040901(R) (2019).
[54] E. Agoritsas and J. Barés (unpublished).
[55] E. Agoritsas, V. Lecomte, and T. Giamarchi, Static fluctuations of a thick one-dimensional interface in the 1+1 directed polymer formulation, Phys. Rev. E **87**, 042406 (2013).
[56] E. Agoritsas, R. García-García, V. Lecomte, L. Truskinovsky, and D. Vandembroucq, Driven interfaces: From flow to creep through model reduction, J. Stat. Phys. **164**, 1394 (2016).
[57] P. Charbonneau, J. Kurchan, G. Parisi, P. Urbani, and F. Zamponi, Fractal free energy landscapes in structural glasses, Nat. Commun. **5**, 3725 (2014).
[58] I. Regev, T. Lookman, and C. Reichhardt, Onset of irreversibility and chaos in amorphous solids under periodic shear, Phys. Rev. E **88**, 062401 (2013).
[59] J. D. Paulsen, N. C. Keim, and S. R. Nagel, Multiple transient memories in experiments on sheared non-Brownian suspensions, Phys. Rev. Lett. **113**, 068301 (2014).